Solid State Voltammetry of an Anthraquinone Molten Salt

Mary Elizabeth Williams[†] and Royce W. Murray*

Kenan Laboratories of Chemistry, University of North Carolina, Chapel Hill, North Carolina 27599-3290

Received: July 28, 1999; In Final Form: September 29, 1999

The solid-state voltammetries of the two reduction steps of a novel redox polyether hybrid—an anthraquinone molten salt (triethyl(MePEG350)ammonium anthraquinone sulfonate, ($Et_3NMePEG350^+$)($AQSO_3^-$))—and its disulfonated analogue, are reported. Multiple effects on charge transport rates are encountered. Currents for the first reduction step are enhanced by electron self-exchange charge transport, whereas currents for the second reduction wave are greater than 10-fold smaller. The relative charge transport rates of the two reductions are examined as a function of temperature and of incrementally replacing the $AQSO_3^-$ anion in the melt with the electroinactive BF_4^- anion. An analysis that includes ionic conductivity measurements shows that the apparent charge transport rate of the second anthraquinone reduction is attenuated primarily as a result of ionic migration of the products of comproportionation reactions occurring in the diffusion layer.

As part of a long-term interest in electron-transfer dynamics in semi-solid-state materials,[1] we recently described a new approach to the synthesis of molten salts that are redox polyether hybrids.[2] Using a polyether-substituted *tetra*-alkylammonium cation (triethyl(MePEG-350)ammonium, $Et_3NMePEG350^+$) as the "tailed counterion" of redox anions such as anthraquinone mono- and disulfonate, produces highly viscous, electroactive molten salts.[2] MePEG-350 stands for poly(ethylene oxide) monomethyl ether, MW = 350; the structures of the sulfonated anthraquinones and polyether cations are as shown below.

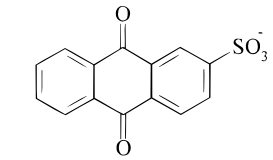

$(AQSO_3)^{1-}$

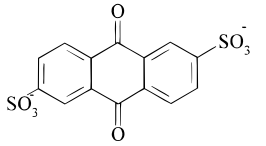

$(AQ(SO_3)_2)^{2-}$

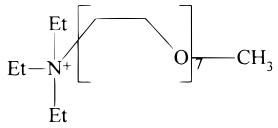

$(Et_3NMePEG\text{-}350)^{1+}$

These materials differ from melts used in our earlier studies[1] of electron transfer, in which the polyether was covalently attached to the redox moiety. The new "tailed counterion" melts are more easily prepared and are an attractive route to expanding the available library of model amorphous semi-solids, for use, among others, in investigating electron transfers in semi-solid-state materials.[2,3]

This paper describes solid state voltammetry from which electron transfer dynamics associated with the two sequential, one-electron reduction reactions of sulfonated anthraquinone ions are assessed. This redox system is the first detailed example of electron transfers in an undiluted melt prepared by association of a redox anion with a polyether-tailed countercation ($Et_3NMePEG350^+$). In another report,[3] we describe electron transfers in melts fashioned from cationic metal complexes using polyether-tailed counteranions.

Experimental Section

Chemicals. Poly(ethylene oxide) monomethyl ether (M_N = 350, MePEG-350, Aldrich) was dried in a vacuum oven at 70 °C for a minimum of 24 h prior to use. Triethylamine and pyridine were dried with activated alumina. Other chemicals were used as received.

Synthesis. Preparation of the Cl^- salt of triethyl(MePEG350)-ammonium polyether cation, abbrev. $(Et_3NMePEG350)^+$, and the melt that this cation forms with anthraquinone-2-sulfonate, abbrev. ($Et_3NMePEG350$)($AQSO_3$), was described previously.[2] A melt of a *di*sulfonated anthraquinone was also prepared as follows. Anthraquinone-2,6-disulfonate disodium salt (Aldrich) was dissolved in hot water and, by reaction with silver nitrate, precipitated as its silver salt. After cooling the mixture to precipitate the anthraquinone disulfonate disilver salt, the solid was filtered and rinsed with copious amounts of water (18 MΩ, Barnstead). A 50% molar excess suspension of anthraquinone disulfonate disilver salt was then stirred in an aqueous solution containing ($Et_3NMePEG350$)(Cl), giving a mixture of solid silver chloride, excess (insoluble) anthraquinone disulfonate disilver salt, and dissolved anthraquinone disulfonate polyether salt, $(Et_3NMePEG350)_2(AQ(SO_3)_2)$. The solids were removed by filtration and the water by rotary evaporation, leaving a clear yellow, viscous oil. ^1H NMR of the molten salt $(Et_3NMePEG350)_2(AQ(SO_3)_2)$ in $CDCl_3$: δ (ppm) 1.35 (t, 18H); 3.3−3.7 (m, 70H); 3.9 (m, 4H); 8.2−8.3 (m, 4H); 8.7 (s, 2H).

The ($Et_3NMePEG350$)(BF_4) salt was prepared by neutralization of ($Et_3NMePEG350$)(OH) with a dilute solution of HBF_4 according to a previously published procedure.[2]

The anthraquinone melts and ($Et_3NMePEG350$)(BF_4) were stored in a drybox prior to use. Mixtures of ($Et_3NMePEG350$)-($AQSO_3$) and ($Et_3NMePEG350$)(BF_4) were prepared by weighing the desired amount of each material in the drybox and then co-dissolving them in acetone to ensure complete mixing. The

[†] Present address: Department of Chemistry, Northwestern University, Evanston, IL 60201.

10.1021/jp992643a CCC: $18.00
Published on Web 11/03/1999

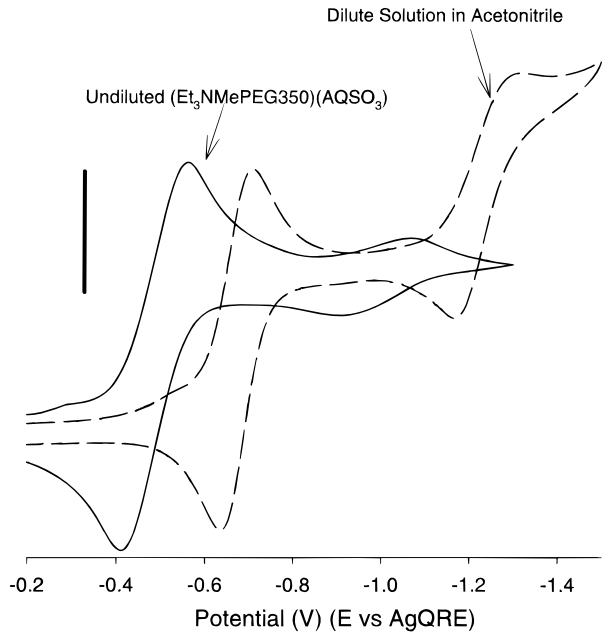

Figure 1. (A) Cyclic voltammogram of $(Et_3NMePEG350)(AQSO_3)$ as a dilute acetonitrile solution (- - -) (2 mM), with 0.1 M tetrabutylammonium perchlorate supporting electrolyte, and using a 50 μm radius Pt disk electrode and potential scan rate of 100 mV/s. Scale bar is 5 μA. (B) Cyclic voltammogram of the undiluted $(Et_3NMePEG350)(AQSO_3)$ melt (—), under vacuum at 45 °C, using a 13.5 μm radius Pt disk working electrode and a potential scan rate of 10 mV/s. Scale bar is 5 nA.

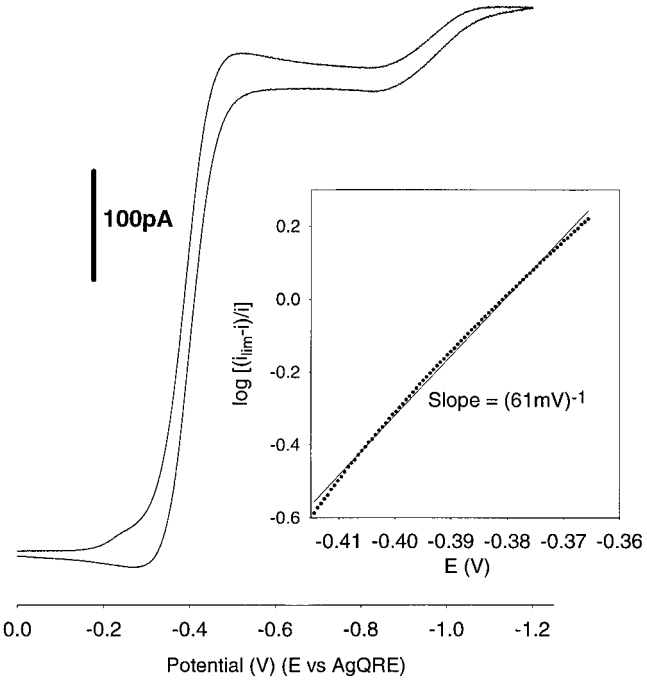

Figure 2. Cyclic voltammetry of pure $(Et_3NMePEG350)(AQSO_3)$ melt using a 2.6 μm radius Pt working electrode and a potential scan rate of 2 mV/s, under vacuum at 40 °C. The inset is a plot of $\log[(i_{LIM} - i)/i]$ versus potential for the first reduction wave, with linear regression.

acetone was flash-evaporated, leaving pale yellow oils that were dried and stored under inert atmosphere.

Electrochemistry. Solid state voltammetry was performed using a microdisk assembly containing the exposed tips of a 13 μm radius Pt working electrode, a 0.55 mm diameter Pt counter electrode, and a 22 gauge Ag quasi-reference electrode.[4] Films of electroactive melt (ca. 5 mm thick) were cast onto the assembly, placed under vacuum and dried at 70 °C for at least 24 h. All voltammetric measurements were made under active vacuum. The temperature of the cell was maintained with a Neslab model RTE-140 circulating bath and measured with a thermocouple located at the cell wall. Data were collected using a low current potentiostat[5] with computer data acquisition and control.[6]

Ionic conductivity was measured by ac impedance spectroscopy using a Solartron model SI 1287 electrochemical interface and SI 1260 impedance/gain phase analyzer. A potential waveform consisting of an ac amplitude of 20 mV and a dc bias of 0 V, and a frequency sweep from 1 MHz to 10 Hz was applied across the fingers of an interdigitated array electrode (IDA, 50 pairs of Pt electrodes, each 3 μm wide, 1 mm long, 0.2 μm high, and separated by 2 μm).[7] The ionic resistance of the melt is taken from the intercept of the real impedance axis in the semicircular complex impedance plot and is converted to ionic conductivity using the known cell constant[8] of the IDA, 0.117 cm^{-1}. The films were cast onto the IDA and dried under vacuum at 40 °C for 48 h. Temperature was maintained using a Lakeshore model 330 autotuning temperature controller. Reported values are the average of at least three measurements.

Results and Discussion

Solid State Voltammetry. Examples of cyclic voltammetry of a dilute (2 mM) solution of $(Et_3NMePEG350)(AQSO_3)$, and as an undiluted molten salt are shown in Figure 1. As a dilute acetonitrile solution, $(Et_3NMePEG350)(AQSO_3)$ displays (- - -) two well-defined reduction waves, of similar peak current, at formal potentials of −0.7 and −1.25 V; these correspond to the one-electron $(AQSO_3)^{1-/2-}$ and $(AQSO_3)^{2-/3-}$ reductions, respectively. The corresponding reduction reactions in the undiluted, pure melt (Figure 1 (—)) appear at −0.5 and −1.0 V (vs Ag quasi-reference electrode), with nearly the same potential separation. The currents observed in the pure melt are ca. 10^3 smaller than those in acetonitrile, despite the ca. 10^3 lower concentration (1.66 M vs 0.002 M) of the latter. The small currents are a familiar observation in solid state voltammetry[1-3] and arise from the much smaller apparent diffusion rates (D_{APP}) in the semi-solid state.

The striking aspect of Figure 1 (—) is that currents for the second reduction wave in the $(Et_3NMePEG350)(AQSO_3)$ melt are much smaller than for the first. The first reduction wave currents are not accentuated by anthraquinone-mediated reduction of dioxygen impurities,[9] since the voltammetry is done under active vacuum and the reduction wave is chemically reversible. The unequal wave heights in Figure 1 (—) arise, instead, from differences in rates of charge transport in the pure melt, as discussed below.

The voltammetry of the undiluted $(Et_3NMePEG350)(AQSO_3)$ melt changes to radial diffusion control (near-steady-state currents) when using a smaller Pt microelectrode and slower potential scan rates, as shown in Figure 2. Steady-state limiting currents at a microdisk electrode of radius r are given by[10]

$$i_{LIM} = 4nFrD_{APP}C \qquad (1)$$

where n is the number of electrons, F the Faraday constant, D_{APP} the charge transport diffusion constant, and C the redox species' concentration. Table 1 lists values of D_{APP} for the first (D_1) and second (D_2) anthraquinone reduction waves, obtained at 27 °C, for the mono- and disulfonated anthraquinone melts. In both melts, we see that D_1 is larger than D_2 by factors of ca. 20-fold.

TABLE 1: Electron Transfer Data for Pure $(Et_3NMePEG350)(AQSO_3)$ and $(Et_3NMePEG350)_2((AQ(SO_3)_2)$ Melts

$(Et_3NMePEG350)^+$ salt	$(AQSO_3)^{1-}$	$(AQ(SO_3)_2)^{2-}$
[AQ] (M)[a]	1.66	1.01
D_1 (27 °C, cm²/s)[b]	1.1×10^{-9}	4.0×10^{-10}
D_2 (27 °C, cm²/s)[c]	5.6×10^{-11}	2.2×10^{-11}
$D_{PHYS,Fc}$ (27 °C, cm²/s)[d]	6.0×10^{-10}	1.6×10^{-10}
k_{EX} (27 °C, M^{-1} s^{-1})[e]	2.2×10^5	8.8×10^4
$E_{A,D1}$ (kJ/mol)[f]	38	44
$E_{A,D2}$ (kJ/mol)[f]	46	52
$E_{A,Fc}$ (kJ/mol)[g]	48	55

[a] Concentration of anthraquinone in the melt, calculated from the density and molecular weight. For $(AQSO_3)$, $\rho = 1.197$ g/mL, MW = 721.4 g/mol; $\delta = 8.97$ Å; for $(AQ(SO_3)_2)$, $\rho = 1.246$ g/mL, MW = 1234.6 g/mol; $\delta = 12.7$ Å. [b] Apparent diffusion coefficient for the first reduction reaction. [c] Apparent diffusion coefficient for the second reduction. [d] Diffusion coefficient for ferrocene, taken as equal to $D_{PHYS,AQ}$. [e] Self-exchange rate constant for the first anthraquinone reduction, using eq 1 and assuming $D_{PHYS,Fc} = D_{PHYS,AQ}$.[11] [f] Activation energy barriers for the first and second anthraquinone reductions, determined from the slopes of the activation plots. [g] Activation energy barrier for the diffusion of ferrocene solute.

Figure 2 (inset) shows a plot of log $[(i_{LIM} - i)/i]$ vs potential for the $(AQSO_3)^{1-/2-}$ wave in Figure 2 (obtained at 40 °C). At that temperature, the slope expected[10] for a reversible electrochemical reaction is 62 mV; the average slope of the slightly curved experimental result is 61 mV, which is very close to the reversible value. An analogous plot for the $(AQSO_3)^{2-/3-}$ wave gives a 161 mV slope, indicating electrochemically quasi-reversible behavior.

Previous studies[1-3] of redox polyether hybrids have shown that the large redox site concentrations and (especially) the slow physical diffusivities of the redox moieties in these undiluted semi-solid materials can lead to current enhancement by electron hopping (self-exchange) reactions in the electrolytically formed mixed valent layer around the electrode. In the present case, then, it might be reasonable to assume, from Figures 1 and 2, that (a) the currents and D_1 values are enhanced for the first, $(AQ)^{1-/2-}$, reduction reaction in the pure melt by a fast electron self-exchange,

$$(AQSO_3)^{1-} + (AQSO_3)^{2-} \rightarrow (AQSO_3)^{2-} + (AQSO_3)^{1-} \quad (2)$$

while (b) currents and D_2 for the second reaction step, $(AQSO_3)^{2-/3-}$, are not analogously (or as much) enhanced, and may simply reflect physical diffusion rates. The first of these assumptions will prove to be correct, and the second, incorrect. The two assumptions can be addressed by measuring the physical diffusion constant $D_{PHYS,AQ}$ of the $(AQSO_3)^{1-}$ reactant in the pure melt. Since this is not possible directly, $D_{PHYS,AQ}$ was determined indirectly using a surrogate diffusant, ferrocene, dissolved in the anthraquinone melt at 1−5 mM concentrations. When the ferrocene is sufficiently dilute, its own electron self-exchange reaction rate becomes unimportant, as evidenced[11] by the concentration-independence of the diffusion constants obtained. The results, shown in Table 1 as $D_{PHYS,Fc}$, are 6×10^{-10} and 1.6×10^{-10} cm²/s in the mono- and disulfonated anthraquinone melts, respectively. These numbers can be viewed as upper limits of the actual ($D_{PHYS,AQ}$) values of the sulfonated anthraquinones (given the smaller size of the ferrocene surrogate), but a large difference is not expected. The $D_{PHYS,AQ}$ results are illuminating, showing that D_1 is larger than $D_{PHYS,AQ}$, in concordance with assumption a above, whereas D_2 is much smaller (8−10 times) than $D_{PHYS,AQ}$, a result quite inconsistent with assumption b. That is, the first reduction wave is (mildly)

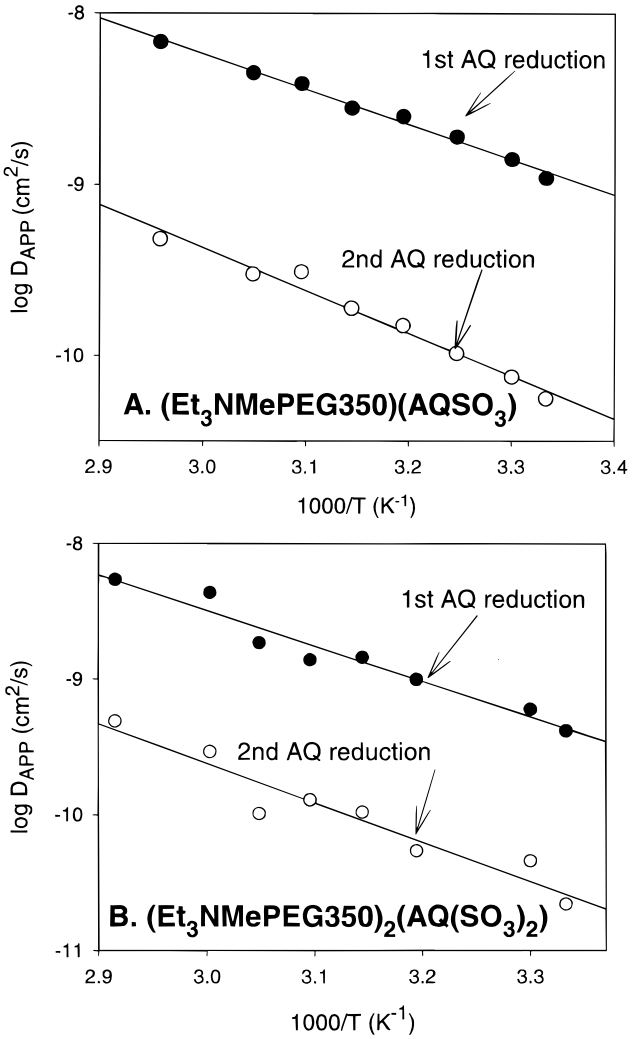

Figure 3. Activation plots of D_{APP} for the first (●) and second (○) reductions in the undiluted (A) $(Et_3NMePEG350)(AQSO_3)$ and (B) $(Et_3NMePEG350)_2(AQ(SO_3)_2)$ molten salts, with linear regression.

enhanced by reaction 2, but some additional factor must intervene to *depress* currents for the second reduction to values far below those expected for simple physical diffusion control.

Focusing first on the enhanced first reduction reaction currents, we draw upon the Dahms−Ruff equation,[12] in which the measured apparent diffusion coefficient D_{APP} is, in a hypothetical cubic lattice model (of the undiluted melt redox sites), the sum of $D_{PHYS,AQ}$ and a term representing the dynamics of the electron self-exchange reaction,

$$D_{APP} = D_{PHYS,AQ} + \frac{k_{EX}\delta^2 C}{6} \quad (3)$$

where k_{EX} is the electron self-exchange rate constant in the melt and δ is the center-to-center charge transfer distance. Taking the $D_{PHYS,AQ} = D_{PHYS,Fc}$ estimate in Table 1, k_{EX} is calculated to be 2×10^5 M^{-1} s^{-1} for reaction 2 in the $(Et_3NMePEG350)(AQSO_3)$ melt and 9×10^4 M^{-1} s^{-1} for the comparable reaction in the $(Et_3NMePEG350)_2(AQ(SO_3)_2)$ melt. (Percolative effects on electron hopping rates are not expected to be important because of the relatively large physical diffusion rates and relatively undiluted anthraquinone concentrations in these melts.[13])

Results for D_1 and D_2 as a function of temperature are shown in Figure 3A, for $(Et_3NMePEG350)(AQSO_3)$, and Figure 3B,

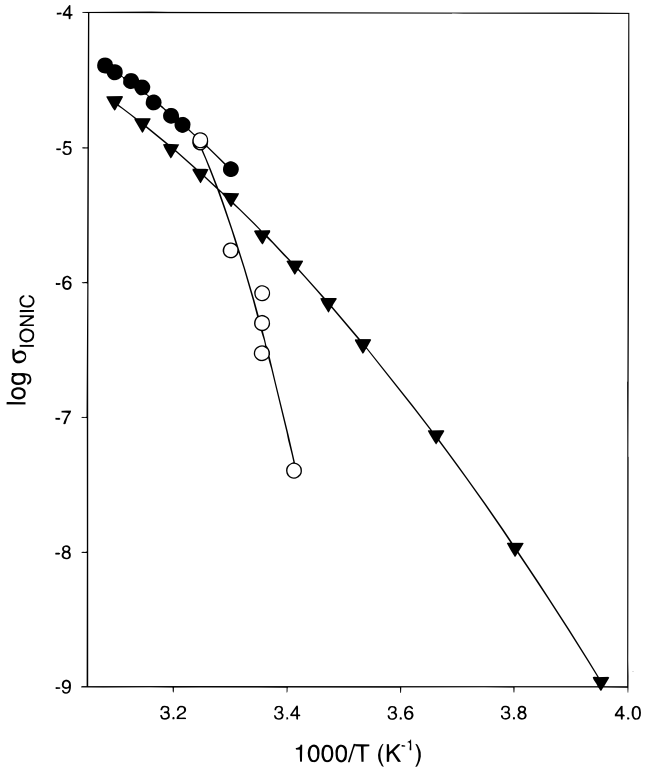

Figure 4. Activation plots of σ_{IONIC} for the $(Et_3NMePEG350)(AQSO_3)$ ((●), above T_C; (○), below T_C) and $(Et_3NMePEG350)_2(AQ(SO_3)_2)$ (▲) molten salts.

for $(Et_3NMePEG350)_2(AQ(SO_3)_2)$. Table 1 gives activation barrier energies, E_{A,D_1} and E_{A,D_2}, derived from the slopes of these plots; that for the disulfonated anthraquinone melt is 7−8 kJ/mol larger than the monosulfonated one. Since D_1 is mainly determined by the electron transfer kinetics, the larger barrier energy in the case of E_{A,D_1} for the disulfonated anthraquinone melt reaction, $(AQ(SO_3)_2)^{2-/3-}$, means that either the reactant is in some way stabilized relative to product, such as by $\{(Et_3NMePEG350)^+\}\{(AQSO_3)^{2-}\}$ ion-pairing, or the barrier energy has been elevated in some other way. (The difference in the D_{PHYS} activation barriers (as measured by $E_{A,Fc}$, Table 1) in the two melts may also contribute to the difference between E_{A,D_1} and E_{A,D_2}). There is also a 7−8 kJ/mol difference between D_1 and D_2, in both melts; the reason for this difference is tenuous given the unresolved kinetic character of D_2.

We turn next to ionic conductivity measurements, which will aid further understanding of D_1 and analysis of the depressed values of D_2.

Ionic Conductivity of Pure Melts. The temperature dependencies of the ionic conductivities, σ_{IONIC}, of the undiluted monosulfonated (●,○) and disulfonated (▲) anthraquinone melts are shown in Figure 4. σ_{IONIC} of the $(Et_3NMePEG350)_2(AQ(SO_3)_2)$ and $(Et_3NMePEG350)(AQSO_3)$ melts are 3.1×10^{-6} and 5.4×10^{-6} S/cm at 27 °C, respectively. The σ_{IONIC} activation plot for the $(Et_3NMePEG350)(AQSO_3)$ (●,○) melt drops off sharply below 27 °C; differential scanning calorimetry measurements show that this material exhibits a crystallization transition, T_C, at that temperature. Crystallizations have been observed in other redox polyether hybrids but are not common;[14] crystallization is not seen in the disulfonated anthraquinone melt. The data reported for σ_{IONIC} and D_1 and D_2 are all taken at $T >$ 27 °C, where $(Et_3NMePEG350)(AQSO_3)$ is an amorphous melt phase.

The activation plots for σ_{IONIC} (Figure 4) are curved (more obviously so for $(Et_3NMePEG350)_2(AQ(SO_3)_2)$. The curvature,

TABLE 2: Ionic Conductivity Data for Pure $(Et_3NMePEG350)(AQSO_3)$ and $(Et_3NMePEG350)_2(AQ(SO_3)_2)$ Melts

$(Et_3NMePEG350)^+$ salt	$(AQSO_3)^{1-}$	$(AQ(SO_3)_2)^{2-}$
[AQ] (M)[a]	1.66	1.01
$[Et_3NMePEG350]^+$ [b](M)	1.66	2.02
σ_{IONIC} (27 °C, S/cm)	5.4×10^{-6}	3.1×10^{-6}
$E_{A,ION}$ (kJ/mol)[c]	66	71
D_{PHYS,Et_3N} (27 °C, cm^2/s)[d]	2.7×10^{-10}	9.1×10^{-11}
D_{PHYS,Et_3N} (27 °C, cm^2/s)[e]	4.4×10^{-10}	1.4×10^{-10}

[a] Concentration of anthraquinone in melt as determined from measured density and given molecular weight. [b] Concentration of $(Et_3NMePEG350)^+$ cation in melt. [c] Activation energy barrier for ionic conductivity, determined from the average slope of the activation plot over the temperature range $T \geq 30$ °C. [d] Calculated diffusion coefficient of the $(Et_3NMePEG350)^+$ cation, using eq 4 and assuming $D_{PHYS,AQ} = D_{PHYS,Fc}$. [e] Calculated diffusion coefficient of the $(Et_3NMePEG350)^+$ cation, using eq 4 and assuming equal diffusivities for all ions present.

as mentioned before,[1c] is thought to reflect physical coupling of the ion motions with polyether segmental motions. The D_{APP} plots for the first reduction step in Figure 3 are linear, reflecting the lower relative importance of physical transport in electron transfers, again as seen before.[1c] The activation barrier energies for σ_{IONIC}, given in Table 2 ($E_{A,ION}$), are much larger than the electron transfer barrier energies (Table 1, $E_{A,D1}$) which is also a typical result for redox polyether hybrids.

The physical diffusivity (D_{PHYS,Et_3N}) of the tailed cation $(Et_3NMePEG350)^+$ can be estimated from the σ_{IONIC} values using the equation[15]

$$\sigma_{IONIC} = \frac{F^2}{RT}(z_{Et_3N}{}^2 D_{PHYS,Et_3N} C_{Et_3N} + z_{AQ}{}^2 D_{PHYS,AQ} C_{AQ}) \quad (4)$$

in which z and C are the charges and concentrations of the $(Et_3NMePEG350)^+$ cation (Et_3N) and the anthraquinone anion (AQ). Table 2 gives resulting D_{PHYS,Et_3N} values based on taking $D_{PHYS,AQ} = D_{PHYS,Fc}$, and on an alternative assumption that $D_{PHYS,Et_3N} = D_{PHYS,AQ}$ (i.e., the anthraquinone anion and its tailed counterion have equal diffusivities). The two calculations give, within a factor of ca. 2-fold, similar values of D_{PHYS,Et_3N}; the latter calculation gives values that in both melts agree with $D_{PHYS,Fc}$ (Table 1). These agreements lend credence to our view that $D_{PHYS,Fc}$ is, in both melts, a reasonably reliable measure of $D_{PHYS,AQ}$, and that the small D_2/D_1 ratios noted above can be reliably interpreted as a combination of an electron transfer enhancement of D_1 with some factor that depresses D_2 to a value smaller than a physical diffusion-controlled one.

Observations of larger first-than-second voltammetric wave currents in two-step electrode reactions are not without precedent. We observed, but did not analyze, a substantially attenuated second wave in the solid state voltammetry of a hybrid perylene−polyether melt.[14d] Smaller second wave currents have been seen[16] in dilute acetonitrile solutions of tetracyanoquinodimethane (TCNQ) containing low electrolyte concentrations and were analyzed in terms of a combined effect of ionic migration and a comproportionation reaction. In highly concentrated organic redox liquids,[17] analysis of observed smaller second waves included electron self-exchange reactions in the first wave as well as ionic migration. The assessment arrived at below is a combination of these previous effects, a theoretical dissection of which is not attempted.

Redox Ion Replacement Experiments. A series of experiments was conducted in which increments of the molten salt $(Et_3NMePEG350)(BF_4)$ were added to the monosulfonated anthraquinone melt, $(Et_3NMePEG350)(AQSO_3)$. (Complete

TABLE 3: Apparent Diffusion Coefficients in a Series of Mixed ($Et_3NMePEG350)(AQSO_3$)/($Et_3NMePEG350)(BF_4$) Melts

$Et_3NMePEG^+$ melt	$[AQSO_3^{1-}]^a$ (M)	$[Et_3NMePEG^+]^b$ (M)	$i_{lim2}/i_{lim1}{}^c$ (27 °C)	D_1 (27 °C)^d (cm^2/s)	D_2 (27 °C)^e (cm^2/s)
$(AQSO_3)^{1-}$	1.66	1.66	0.051	1.1×10^{-9}	5.6×10^{-11}
$(AQSO_3)^{1-} + (BF_4)^-$ [f]	1.43	1.83	0.043	1.2×10^{-9}	5.1×10^{-11}
$(AQSO_3)^{1-} + (BF_4)^-$ [f]	0.93	2.0	0.12	2.6×10^{-9}	3.0×10^{-10}
$(AQSO_3)^{1-} + (BF_4)^-$ [f]	0.75	2.1	0.28	3.3×10^{-9}	9.2×10^{-10}
$(AQSO_3)^{1-} + (BF_4)^-$ [f]	0.45	2.2	0.33	6.3×10^{-9}	2.1×10^{-9}
$(AQSO_3)^{1-} + (BF_4)^-$ [f]	0.17	2.3	0.53	9.8×10^{-9}	5.2×10^{-9}
$(AQSO_3)^{1-} + (BF_4)^-$ [f]	0.026	2.4	0.50	2.6×10^{-8}	1.3×10^{-8}

[a] Concentration of anthraquinone in melt. [b] Total polyether cation in mixed ($Et_3NMePEG350)(AQSO_3$)/($Et_3NMePEG350)(BF_4$) melt. [c] Ratio of the two limiting currents. [d] Apparent diffusion coefficient for the first reduction, $(AQSO_3)^{1-/2-}$. [e] Apparent diffusion coefficient for the second reduction, $(AQSO_3)^{2-/3-}$. [f] Mixed melts.

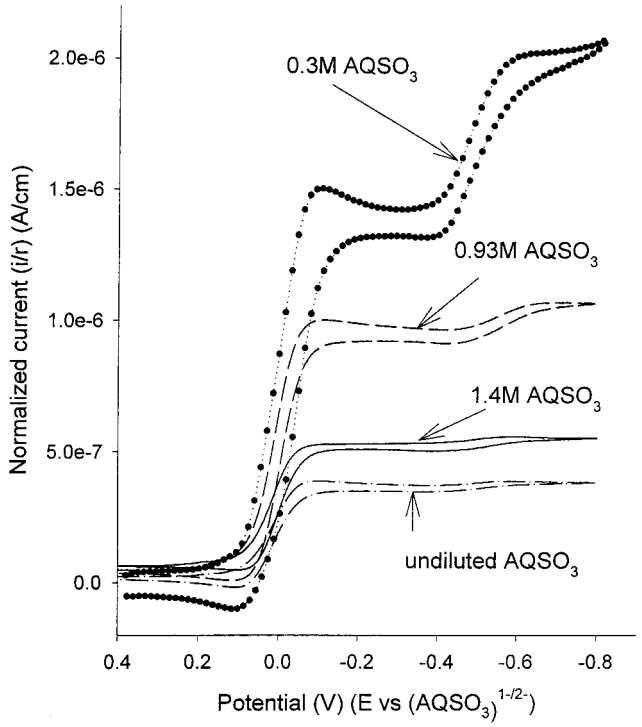

Figure 5. Cyclic voltammograms of ($Et_3NMePEG350)(AQSO_3$) melts containing added ($Et_3NMePEG350)(BF_4$) electrolyte, with the indicated concentrations of anthraquinone. Currents have been normalized to the radius of the Pt microdisk working electrode (which ranged from 2.6 to 13.5 μm), and the potential scale is referenced to the first reduction half-wave potential.

mixing was ensured by codissolution of the two materials in the casting solvent.) Addition of ($Et_3NMePEG350)(BF_4$) has the effect of replacing (per unit volume) the monosulfonated anthraquinone anion with the BF_4^- anion, decreasing the concentration of the former (see Table 3), and, since the BF_4^- anion has a smaller molar volume, increasing the $(Et_3NMePEG350)^+$ cation concentration. The increased polyether content of the (otherwise undiluted) mixed melt can be expected to "plasticize" the melt somewhat, increasing physical diffusivity and ionic conductivity values. The added ($Et_3NMePEG350)(BF_4$) is also expected to act as a "supporting electrolyte" and reduce the role of ionic migration of the sulfonated anthraquinone anion (and its reduction product) in supporting ionic charge flow through the melt in response to the voltammetry. This last point was, in fact, the goal of the ($Et_3NMePEG350)(BF_4$) addition.

Voltammetry of mixed melts (at 55 °C) is shown in Figure 5. Adding ($Et_3NMePEG350)(BF_4$) has two effects; the currents increase for both reduction waves but more so for the second wave, causing the limiting currents for the two waves to become more equal. Ratios of limiting currents (i_{LIM2}/i_{LIM1}) and values of D_1 and D_2 are given in Table 3, and the ionic conductivities of several of the melt mixtures in Table 4. Table 4 also presents D_{PHYS,Et_3N} and $D_{PHYS,AQ}$ diffusivities and values of the transference number t_{AQ} (the fraction of the ionic current carried by the sulfonated anthraquinone anion during electrolysis), calculated using the relation[15]

$$t_{AQ} = \frac{z_{AQ}{}^2 D_{PHYS,AQ} C_{AQ}}{(\sigma_{IONIC} RT/F^2)} \quad (5)$$

The calculated t_{AQ} values range from 0.69 in the pure ($Et_3NMePEG350)(AQSO_3$) melt to 0.05 in the melt to which the largest portion of ($Et_3NMePEG350)(BF_4$) has been added. The large value of t_{AQ} in pure ($Et_3NMePEG350)(AQSO_3$) means that the $(AQSO_3)^{1-}$ reactant carries a substantial fraction of the ionic current flow during the $(AQSO_3)^{1-/2-}$ reduction reaction. The anionic current flow is in a direction away from the melt/electrode interface and thus opposes the diffusive flux of $(AQSO_3)^{1-}$ toward the electrode. This implies that the value of D_1 observed in the pure ($Et_3NMePEG350)(AQSO_3$) melt may have been depressed (by as much as 2-fold, i.e., an improved value of k_{EX} would be $\sim 4 \times 10^5$ M^{-1} s^{-1} for reaction 2 in the pure ($Et_3NMePEG350)(AQSO_3$) melt at 27 °C).

Analysis of The Smaller Second Reduction Wave. We now focus on the behavior of the second anthraquinone reduction wave. The $t_{AQ} = 0.69$ result in the pure ($Et_3NMePEG350)(AQSO_3$) melt signals significant ionic migration of the $(AQSO_3)^{1-}$ reactant and means that the $(AQSO_3)^{2-}$ reaction product will also experience ionic migration *away* from the electrode, *counteracting* its physical diffusion transport rate. The latter circumstance is reminiscent of observations by White et al.,[16] in (dilute) TCNQ solutions in low ionic strength acetonitrile, where currents for the first, $TCNQ^{0/1}$, reduction wave were larger than for the second, $TCNQ^{1-/2-}$, wave. These results were interpreted as reflecting a depression of the second wave currents by a combination of the comproportionation reaction,

$$TCNQ + TCNQ^{2-} \rightarrow 2TCNQ^{1-} \quad (6)$$

and ionic migration of the comproportionation reaction product ($TCNQ^{1-}$) away from the electrode. Theory showed that the effect is maximized when the normalized rate of the comproportionation reaction is large compared to the normalized mass transport rate.

The ($Et_3NMePEG350)(AQSO_3$) melt is analogous to the TCNQ case[16] in that the current ratio i_{LIM2}/i_{LIM1} increases when electrolyte is added, and the $(AQSO_3)^{2-}$ reaction product is anticipated to experience ionic migration away from the electrode. Additionally, in the second anthraquinone reduction wave, the comproportionation reaction[18]

$$AQSO_3{}^{1-} + AQSO_3{}^{3-} \rightarrow 2AQSO_3{}^{2-} \quad (7)$$

TABLE 4: Ionic Conductivity of ($Et_3NMePEG350$)($AQSO_3$) Melts Containing Added ($Et_3NMePEG350$)(BF_4) Electrolyte (27 °C)

$Et_3NMePEG^+$ Melt	[AQ] (M)	[Et_3N] (M)	σ_{IONIC} (Scm^{-1})[a]	$D_{PHYS,Et3N}$ (cm^2/s)[b]	$D_{PHYS,AQ}$ (cm^2/s)[b]	t_{AQ}[c]
($Et_3NMePEG350$)($AQSO_3$)	1.66	1.66	5.4×10^{-6}	2.7×10^{-10}	6.0×10^{-10}	0.69
$(AQSO_3)^{1-} + (BF_4)^-$[d]	0.93	2.0	1.6×10^{-5}	6.7×10^{-10}	1.5×10^{-9}	0.33
$(AQSO_3)^{1-} + (BF_4)^-$[d]	0.45	2.2	1.9×10^{-5}	7.2×10^{-10}	1.6×10^{-9}	0.14
$(AQSO_3)^{1-} + (BF_4)^-$[d]	0.17	2.3	1.8×10^{-5}	6.6×10^{-10}	1.5×10^{-9}	0.05

[a] Ionic conductivity measured at 27 °C by ac impedance. [b] Diffusion coefficient for $(Et_3NMePEG350)^+$ cation calculated using eq 4 and assuming that the ratio $D_{PHYS,AQ}/D_{PHYS,Et3N}$ in the mixed melts is the same factor that it was in the pure ($Et_3NMePEG350$)($AQSO_3$) melt (Table 2), i.e., $D_{PHYS,AQ} = D_{BF_4} = 2.2\ D_{PHYS,Et3N}$. [c] Transference number of anthraquinone anion using eq 5 with $D_{PHYS} = D_{AQ}$. [d] Mixed melts, containing added ($Et_3NMePEG350$)(BF_4).

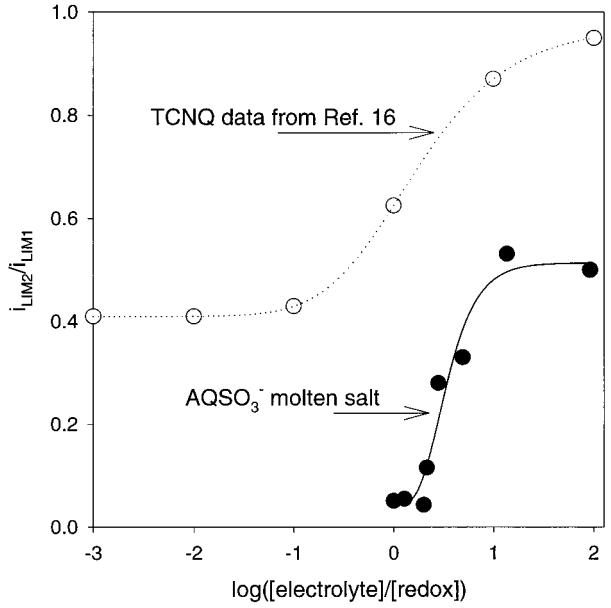

Figure 6. Plot of the ratio of limiting currents for the two anthraquinone reductions (i_{LIM2}/i_{LIM1}) versus the ratio of the total $(Et_3NMePEG350)^+$ electrolyte to anthraquinone concentrations (●). Also shown is data from ref 16 for 1 mM TCNQ in acetonitrile at varying concentrations of tetrabutylammonium perchlorate supporting electrolyte (○).

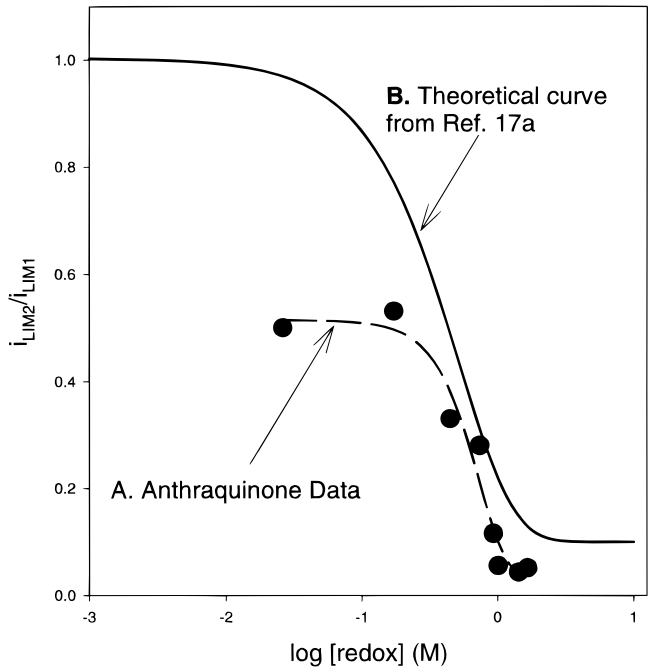

Figure 7. (A) Plot of the ratio of limiting currents (i_{LIM2}/i_{LIM1}) versus anthraquinone concentration (●). (B) Theoretical working curve (—) from ref 17a for $k_{EX}\delta^2/6D_{PHYS} = 7.7$ and supporting electrolyte concentration 0.5 M.

can be expected to occur in the diffusion layer around the electrode. Reaction 7 should have a very large rate constant, given its equilibrium constant of $\sim 10^9$ that can be deduced from the 520 mV separation between the first and second wave formal potentials (Figure 1).

Figure 6 compares the TCNQ data[16] to the ($Et_3NMePEG350$)-($AQSO_3$) results of Table 3. The lower [electrolyte]/[redox] ratios used in the TCNQ solutions are inaccessible in the anthraquinone melts, since the lower limit there—the undiluted ($Et_3NMePEG$-350)($AQSO_3$) melt—has equal cation and anion concentrations. Both systems display a sharp effect of electrolyte ion concentration. The depression of i_{LIM2}/i_{LIM1} in the anthraquinone melt is, however, much more pronounced than either the TCNQ results or any of the theoretical simulations presented;[16] also i_{LIM2}/i_{LIM1} in the melt does not go to unity at high electrolyte concentration. We conclude from this comparison that the ionic migration-comproportionation reaction combination[16] cannot, alone, account for the voltammetric behavior of the anthraquinone melt.[19]

The Figure 6 simulations[16] did not include electron self-exchange (such as reaction 2) as a charge transport mode, and the larger ionic charge of the $(AQSO_3)^{2-}$ species should additionally invoke a more pronounced ionic migration effect. In fluid redox media that are highly concentrated, electron-transfer reactions such as reaction 2 can act to enhance charge transfer, and this has been reported[17] in the voltammetry of nitrobenzene and 4-cyanopyridine. Currents for the first of the two sequential reductions in the latter media were larger than the second at the highest redox concentrations but became equal at lower concentrations. Figure 7 shows a theoretical response developed[17] that incorporates effects of both electron transfer-based charge transport in the first wave (enhancing it) and the ionic migration-comproportional reaction acting on the second (depressing it). The Figure 7 curve is for the parameter $k_{EX}\delta^2/6D_{PHYS} = 7.7$ (where the symbols are the same as in eq 3 above). The amount of depression of i_{LIM2}/i_{LIM1} is predicted[17] to increase as $k_{EX}\delta^2/6D_{PHYS}$ increases. Figure 7 also shows the i_{LIM2}/i_{LIM1} data of Table 3. In the pure ($Et_3NMePEG350$)-($AQSO_3$) melt, based on the above analysis of the first reduction wave, $k_{EX}\delta^2/6D_{PHYS} \approx 1$, which is smaller than that for the theoretical curve in Figure 7, suggesting that a larger i_{LIM2}/i_{LIM1} ratio should be expected. However, the observed i_{LIM2}/i_{LIM1} ratio in the pure melt is in fact smaller (0.05). Additionally, i_{LIM2}/i_{LIM1} in the mixed melt does not go to unity at high concentrations of added ($Et_3NMePEG350$)(BF_4).

The Figure 7 analysis comes close to explaining the anthraquinone voltammetry, but as noted just above, does not do so quantitatively. We speculate that a combination of (at least) two differences between the fluid redox liquids[17] and the ($Et_3NMePEG350$)($AQSO_3$) melt causes the observed divergence. First, the theoretical curve in Figure 7 anticipates that current-enhancing effects of electron transfer-based charge transport vanish as the redox liquid is diluted. That this does not, apparently, transpire in the mixed ($Et_3NMePEG350$)-

$(AQSO_3)$/$(Et_3NMePEG350)(BF_4)$ melt (Figure 5 and Table 3) implies that the effects of electron-transfer dynamics of reaction 2 have not been completely suppressed and that k_{EX} increases in the (more fluid) mixed melt by an amount roughly offsetting the lowering of the $(AQSO_3)^-$ concentration. We also note that in the diluted mixed melt, in which, for example, $(AQSO_3)^-$ concentration has been lowered 10-fold to 0.17 M, D_1 is about 10-fold larger than D_{PHYS,Et_3N}, meaning that if electron self-exchanges act to enhance i_{LIM1}, *electronic* migration would be additionally present and would accentuate i_{LIM1} even further. (Electronic migration refers[20] to electron self-exchange transport rates exceeding charge compensating ionic transport, setting up a potential gradient that accelerates the electron self-exchanges.) Application of a theory for electronic migration in fixed-site redox polymers (an obvious approximation to the present material) to correct for this effect produces a value of $k_{EX} \approx 1.6 \times 10^5\ M^{-1}\ s^{-1}$.

The increase of k_{EX} in the diluted melts (relative to the pure melt) is a somewhat surprising result, and we emphasize the speculative nature[21] of the above correction of k_{EX}. Second, the greater depression of the i_{LIM1}/i_{LIM2} ratio in the pure melt, relative to the theoretical prediction in Figure 7, may reflect (at least in part, from the Figure 6 comparisons) the greater ionic charge of the $(AQSO_3)^-$ ion, as noted earlier.

Acknowledgment. This work was supported by grants from the U.S. Department of Energy and the National Science Foundation. M.E.W. gratefully acknowledges a fellowship from the American Chemical Society Division of Analytical Chemistry sponsored by Eastman Chemical Company.

References and Notes

(1) (a) Velasquez, C. S.; Hutchinson, J. E.; Murray, R. W. *J. Am. Chem. Soc.* **1993**, *115*, 7896. (b) Velasquez, C. S.; Murray, R. W. *J. Electroanal. Chem.* **1995**, *396*, 349. (c) Williams, M. E.; Masui, H.; Long, J. W.; Malik, J.; Murray, R. W. *J. Am. Chem. Soc.* **1997**, *119*, 1997. (d) Williams, M. E.; Lyons, L. J.; Long, J. W.; Murray, R. W. *J. Phys. Chem.* **1997**, *101*, 7584.

(2) Dickinson, E. V.; Williams, M. E.; Hendrickson, S. M.; Masui, H.; Murray, R. W. *J. Am. Chem. Soc.* **1999**, *121*, 613.

(3) Dickinson, E. V.; Masui, H.; Williams, M. E.; Murray, R. W. Submitted for publication.

(4) Longmire, M. L.; Watanabe, M.; Zhang, H.; Wooster, T. T.; Murray, R. W. *Anal. Chem.* **1990**, *62*, 747.

(5) Woodward, S. Electronics Consultant, University of North Carolina at Chapel Hill.

(6) Terrill, R. H. University of North Carolina at Chapel Hill, data acquisition software.

(7) The IDA was generously provided by O. Niwa, Nippon Telephone and Telegraph.

(8) Kissinger, P. T.; Heineman, W. R. *Laboratory Techniques in Electroanalytical Chemistry*; M. Dekker: New York, 1984; p 243.

(9) Ingram, R. S. University of North Carolina, unpublished results.

(10) Wightman, R. M.; Wipf, D. O. In *Electroanalytical Chemistry*; Bard, A. J., Ed.; Marcel Dekker: New York, 1980; Vol. 15.

(11) D_{Fc} did not vary as a function of concentration of ferrocene. In the $(Et_3NMePEG350)(AQSO_3)$ melt, reported D_{Fc} is the average of: 1.1 mM Fc, D_{Fc} (27 °C) = 5.91×10^{-10} cm^2/s; 4.66 mM Fc, D_{Fc} (27 °C) = 6.24×10^{-10} cm^2/s; 5.8 mM Fc, D_{Fc} (27 °C) = 5.82×10^{-10} cm^2/s. Reported D_{Fc} in $(Et_3NMePEG350)_2(AQ(SO_3)_2)$ melt is for 2.6 mM Fc. The voltammetry and ionic conductivity of the anthraquinone melt also did not change upon addition of ferrocene.

(12) Majda, M. In *Chemical Design of Electrode Surfaces*; Murray, R. W., Ed; Wiley: New York, 1992; pp 159−206.

(13) Long, J. W.; Velasquez, C. S.; Murray, R. W. *J. Phys. Chem.* **1996**, *100*, 5492.

(14) (a) Partial crystallinity has been observed in other redox polyether melts. (b) Pinkerton, M. J.; Le Mest, Y.; Zhang, H.; Watanabe, M.; Murray, R. W. *J. Am. Chem. Soc.* **1990**, *112*, 3730. (c) Long, J. W.; Kim, I.-K.; Murray, R. W. *J. Am. Chem. Soc.* **1997**, *119*, 11510. (d) Williams, M. E.; Murray, R. W. *Chem. Mat.* **1998**, *10*, 3603.

(15) Bard, A. J.; Faulkner, L. R. *Electrochemical Methods, Fundamentals and Applications*; John Wiley & Sons: New York, 1980.

(16) (a) Norton, J. D.; Benson, W. E.; White, H. S.; Pendley, B. D.; Abruna, H. D. *Anal. Chem.* **1991**, *63*, 1909. (b) Amatore, C.; Paulson, S. C.; White, H. S. *J. Electroanal. Chem.* **1997**, *439*, 173.

(17) (a) Norton, J. D.; Anderson, S. A.; White, H. S. *J. Phys. Chem.* **1992**, *96*, 3. (b) Morris, R. B.; Fischer, K. F.; White, H. S. *J. Phys. Chem.* **1988**, *92*, 5306. (c) Malmsten, R. A.; White, H. S. *J. Electrochem Soc* **1986**, *133*, 1067.

(18) (a) Strojek, J. W.; Kuwana, T.; Feldberg, S. W. *J. Am. Chem. Soc.* **1968**, *90*, 1353. (b) Winograd, N.; Kuwana, T. *J. Am. Chem. Soc.* **1970**, *92*, 224. (c) Winograd, N.; Kuwana, T. *J. Am. Chem. Soc.* **1971**, *4343*. (d) Andrieux, C. P.; Saveant, J.-M. *J. Electroanal. Chem.* **1970**, *28*, 339. (e) Tsou, Y.-M.; Anson, F. C. *J. Phys. Chem.* **1985**, *89*, 3818. (f) Rongfeng, Z.; Evans, D. H. *J. Electroanal. Chem.* **1995**, *385*, 201. (g) Lehmann, M. W.; Evans, D. H. *Anal. Chem.* **1999**, *71*, 1947.

(19) (a) An alternative explanation for the smaller second anthraquinone reduction wave was suggested by a reviewer, namely kinetically limited formation of an anthraquinone dimer or quinhydrone, such as recently reported[19b] for quinones in dilute solutions. This suggestion is discarded because (i) the melt media lacks the proton source shown to be essential for quinhydrone formation and (ii) the effect of added $(Et_3NMePEG350)(BF_4)$ is not easily understood in the context of quinhydrone formation. (b) Gupta, N.; Linschitz, H. *J. Am. Chem. Soc.* **1997**, *119*, 6384−6391.

(20) (a) Andrieux, C. P.; Saveant, J.-M. *J. Phys. Chem.***1988**, *92*, 6762. (b) For the working curves, the parameters $n/z_c = 1$ and $-(\gamma + 1) = 1$ were used.

(21) Application of electronic migration correct to the k_{EX} in the pure melt produces in comparison an insignificant correction of only about 10%, because there the ratio $D_1/D_{PHYS,\ Et_3N} \approx 1-2$.